

---

# NeuralOM: Neural Ocean Model for Subseasonal-to-Seasonal Simulation

---

Yuan Gao<sup>1\*</sup>, Ruiqi Shu<sup>1\*</sup>, Hao Wu<sup>1\*</sup>, Fan Xu<sup>2</sup>, Yanfei Xiang<sup>1</sup>, Ruijian Gou<sup>3</sup>,  
Qingsong Wen<sup>4</sup>, Xian Wu<sup>5</sup>, Xiaomeng Huang<sup>1†</sup>

<sup>1</sup>Tsinghua University, <sup>2</sup>University of Science and Technology of China,

<sup>3</sup>Ocean University of China, <sup>4</sup>Squirrel Ai Learning, <sup>5</sup>TEG, Tencent  
hxm@tsinghua.edu.cn

## Abstract

Accurate Subseasonal-to-Seasonal (S2S) ocean simulation is critically important for marine research, yet remains challenging due to its substantial thermal inertia and extended time delay. Machine learning (ML)-based models have demonstrated significant advancements in simulation accuracy and computational efficiency compared to traditional numerical methods. Nevertheless, a significant limitation of current ML models for S2S ocean simulation is their inadequate incorporation of physical consistency and the slow-changing properties of the ocean system. In this work, we propose a neural ocean model (NeuralOM) for S2S ocean simulation with a multi-scale interactive graph neural network to emulate diverse physical phenomena associated with ocean systems effectively. Specifically, we propose a multi-stage framework tailored to model the ocean’s slowly changing nature. Additionally, we introduce a multi-scale interactive messaging module to capture complex dynamical behaviors, such as gradient changes and multiplicative coupling relationships inherent in ocean dynamics. Extensive experimental evaluations confirm that our proposed NeuralOM outperforms state-of-the-art models in S2S and extreme event simulation. The codes are available at <https://github.com/YuanGao-YG/NeuralOM>.

## 1 Introduction

Subseasonal-to-Seasonal (S2S) simulation represents a simulation of a dynamic system 2 to 6 weeks in advance [21]. Accurate S2S ocean simulation plays a pivotal role in marine research and activities, yet it remains a significant challenge due to the ocean’s substantial thermal inertia and prolonged time delay [35, 18]. Traditional numerical ocean modeling systems, such as the Mercator Ocean Physical System (PSY4) and Real-Time Ocean Forecast System (RTOFS), rely on physics-driven numerical models to simulate ocean phenomena. These models use supercomputers to solve complex partial differential equations based on current ocean conditions [8]. Although these numerical systems achieve high accuracy, they are computationally expensive and time-consuming, requiring hours of computation even with hundreds of computational nodes. Moreover, enhancing the accuracy of these numerical methods is highly challenging, as they depend significantly on human expertise in understanding the complex physical laws governing the ocean environment.

Machine Learning (ML) provides a new perspective for ocean simulation due to several orders of magnitude faster than traditional numerical methods and high efficiency [20] [12]. Some spatio-temporal prediction algorithms, such as NMO [39], neXtSIM [7], OceanVP [29] focus on regional ocean modeling. And some ML-based task-specific ocean models are proposed, such as ENSO (El Niño/Southern

---

\*Equal Contribution

†Corresponding Author

Oscillation) prediction [11] [3], MJO (Madden Julian Oscillation) prediction [16] [6] [31], and MHWs (Marine Heatwaves) prediction [28] [15] [32]. In recent years, learning from the algorithms of ML-based global atmosphere foundation models [26] [1], ML-based global ocean foundation models have emerged, such as AI-GOMS [40], Xihe [38], and WenHai [5]. Some foundation models achieve better performance than traditional numerical models. However, ML-based global ocean foundation models still face several core challenges: ❶ *Slow-changing processes are hard to model*. Due to substantial thermal inertia and extended time delay of the ocean system, it is difficult to learn the small changes effectively. ❷ *Subseasonal-to-seasonal simulation lacks of adaptive modeling*. Different time scales incorporate multi-scale ocean movements. Focusing on single-scale movement is hard to model consistently with the evolution process of ocean dynamics.

To address these challenges, this work proposes NeuralOM, a neural ocean model for subseasonal-to-seasonal simulation. Specially, to model the ocean’s slowly changing nature, we propose an ocean-specific multi-stage framework to learn large-scale to small-scale characteristics step by step. Under this framework, variables with seasonal periodicity, such as sea salinity, sea temperature, and sea surface height, are first subtracted from the climatology so that the model can better capture subtle changes. Additionally, we introduce a multi-scale interactive messaging module to capture complex dynamical behaviors, such as gradient changes and multiplicative coupling relationships inherent in ocean dynamics, which contributes to the S2S time scale simulation by adaptively modeling multi-scale movements.

The contribution of this work can be summarized as: (1) *Stable Subseasonal-to-Seasonal Ocean Simulation Framework*. We proposed an ocean-specific multi-stage framework tailored for the slow change nature of the ocean dynamic system, which achieves stable ocean simulation at S2S time scale. (2) *Adaptively Modeling of Multi-scale Movements for Ocean Dynamic System*. We propose a multi-scale interactive graph neural network to adaptively model the evolution process of ocean dynamic system. (3) *Competitive Experimental Results*. Extensive experiments demonstrate that our proposed model outperforms state-of-the-art models in S2S and extreme event simulation.

## 2 Related Work

**ML-based Task-specific Ocean Model.** The goal for this type of ocean model is to simulate specific ocean phenomena. Recent achievements includes ENSO (El Niño/Southern Oscillation) prediction [11] [14] [2] [23] [3], MJO (Madden Julian Oscillation) prediction [16] [6] [42] [30] [31], MHWs (Marine Heatwaves) prediction [15] [36] [25] [32], Sea Surface Height anomaly (SSHa) prediction [33] [19]. These models have demonstrated promising performance in comparison to traditional methods. However, several models overlook the interactions between multiple variables, suggesting that ML-based ocean models could potentially achieve enhanced accuracy by incorporating multi-variable interactions across 3D depth levels with a foundation model.

**ML-based Global Ocean Foundation Model.** The global ocean foundation models have significant achievements with higher accuracy and better efficiency than traditional numerical models. AI-GOMS [40] is an ocean foundation model that employs MAE [13] to simulate a multi-layer ocean state. Xihe [38] achieves an eddy-resolving simulation based on the hierarchical transformer. Some research, such as ORCA-DL [10], OCE [34], and DLESyM [4], targets decadal to climate-scale simulation, which indicates tremendous potential of ML-based models in climate simulation. LangYa [41] is a cross-spatiotemporal ocean model with large-language model-based time embedding. Subsequently, WenHai [5] incorporates domain knowledge into Swin Transformer [22] and achieves better performance than the numerical model.

## 3 Method

**Problem Setup** In this work, we formulate ocean simulation as an autoregressive problem. For each time step  $t$ , we use the ocean state and forcing to simulate the next time step ocean state. The ocean state is composed of ocean depth level variables  $\mathbf{O}_t^d$  and surface variables  $\mathbf{O}_t^s$ , while the forcing includes atmosphere surface variables  $\mathbf{F}_t$  and  $\mathbf{F}_{t+1}$ . These components are concatenated along the channel dimension to form the combined input:  $\mathbf{X}_t = [\mathbf{O}_t^d, \mathbf{O}_t^s, \mathbf{F}_t, \mathbf{F}_{t+1}] \in \mathbb{R}^{N \times d}$ , where  $N = H \times W$  represents the number of grid locations, and  $d = d_d + d_s + d_f$  is the total number of input variables. Here,  $d_d$ ,  $d_s$ , and  $d_f$  are the numbers of ocean depth level variables, surface level variables,

and forcing variables, respectively. In our setup, the input contains 101 variables: 92 depth level variables, 1 surface level variable, and 8 forcing variables. The model aims to simulate the next time ocean state  $\hat{\mathbf{O}}_{t+1}$ , given the current input  $\mathbf{X}_t$ , capturing the spatiotemporal evolution of the ocean:  $\hat{\mathbf{O}}_{t+1} = \text{Model}(\mathbf{X}_t; \Theta)$ , where  $\Theta$  denotes the model parameters.  $\hat{\mathbf{O}}_{t+1} = [\hat{\mathbf{O}}_{t+1}^d, \hat{\mathbf{O}}_{t+1}^s] \in \mathbb{R}^{N \times d_o}$ , where  $d_o = d_d + d_s$  is the total number of ocean variables. The training objective is to minimize the relative mean squared error (MSE) between the simulations and the true values across all time steps:  $\min_{\Theta} \frac{1}{T} \sum_{t=0}^{T-1} \frac{\|\hat{\mathbf{O}}_{t+1} - \mathbf{O}_{t+1}\|_2^2}{\|\mathbf{O}_{t+1}\|_2^2}$ . During inference, we employ a rollout strategy to simulate longer sequences. Starting from the initial state  $\mathbf{X}_0$ , the model recursively uses its previous simulations as the next input:  $\hat{\mathbf{O}}_{t+1} = \text{Model}(\hat{\mathbf{X}}_t; \Theta)$ ,  $t = 0, 1, 2, \dots, T - 1$ .

### 3.1 Ocean-specific Multi-stage Framework

Due to its substantial thermal inertia and extended time delay, the ocean changes slowly compared to its original state, making it difficult to effectively learn and capture changes. Therefore, as depicted in Figure 1(a), we propose an ocean-specific multi-stage framework (OMF) to learn small change nature. Specifically, different from previous works such as AI-GOMS, Xihe, and WenHai, we first remove the climatological mean from variables exhibiting strong periodicity before feeding them into the network, thereby directing the model’s attention toward small anomalies:

$$O_t^{\text{periodic}} = O_t^{\text{original}} - O_t^{\text{climatology}}, \quad (1)$$

where,  $O_t^{\text{periodic}}$  denotes periodic ocean variables (sea salinity, sea temperature, and sea surface height),  $O_t^{\text{original}}$  represents the original ocean variables,  $O_t^{\text{climatology}}$  is the climatology calculated by the historical data from 1993 to 2017, exclude from valid and test data. Therefore, the input ocean variables  $O_t = [O_t^{\text{periodic}}, O_t^{u,v}] \in \mathbb{R}^{N \times d_o}$ .  $O_t^{u,v}$  is sea stream velocity. Then, inspired by [24] that intends to reduce step error for scientific data prediction and a multi-step supervised method [37], we adopt a stage-wise learning strategy to sequentially capture the ocean’s gradual evolution. It is worth noting that although the previous works could reduce single-step error for some ideal datasets, they are hard to achieve long-term simulation in complex real-world ocean scenes. In contrast, our proposed OMF focuses on long-term simulation and achieves stable subseasonal-to-seasonal ocean simulation. Specifically, the intermediate results of the next step ocean state  $\hat{O}_{t+1}$  can be acquired using the combined input  $X_t = [O_t, F_t, F_{t+1}] \in \mathbb{R}^{N \times d}$ :

$$\hat{O}_{t+1}^1 = \mathcal{F}_1^M(X_t), \quad (2)$$

where,  $\mathcal{F}_1^M$  is the first model with M-step finetune, which can be trained step by step from the 1-step supervised model. Subsequently, as shown in Figure 1(a), we apply the second model to learn the residue between  $\hat{O}_{t+1}^1$  and  $O_{t+1}$ , thereby getting the intermediate results produced by the second model:

$$\hat{O}_{t+1}^2 = \mathcal{F}_2^N(\hat{O}_{t+1}^1) + \hat{O}_{t+1}^1, \quad (3)$$

where,  $\mathcal{F}_2^M$  is the second model with N-step finetune, which is trained step by step. For the last model:

$$\hat{O}_{t+1} = \mathcal{F}_Q^N(\hat{O}_{t+1}^{Q-1}) + \hat{O}_{t+1}^{Q-1}, \quad (4)$$

where,  $\mathcal{F}_Q^N$  denotes the Qth model with N-step finetune. In our experiment, we set M=6, N=10, and Q=2 as an example to demonstrate that the proposed ocean-specific multi-stage framework could improve the long-term simulation for complex ocean dynamic systems.

## 3.2 Multi-scale Interactive Graph Neural Networks

### 3.2.1 Graph Encoder

Following the previous works [17, 9], we employ the multi-scale graph encoder to map the data from lat-lon grids into a graph structure. The multi-scale graph structure can be defined as:

$$\mathcal{G} = (\mathcal{V}^G, \mathcal{V}, \mathcal{E}_m, \mathcal{E}^{\text{G2M}}, \mathcal{E}^{\text{M2G}}), \quad (5)$$

where,  $\mathcal{V}^G$  represents the set of lat-lon grid nodes, with a total of  $N = H \times W$  nodes;  $\mathcal{V}$  represents the mesh nodes;  $\mathcal{E}_m$  denotes the multi-scale edges, which represents the edge with different lengths;

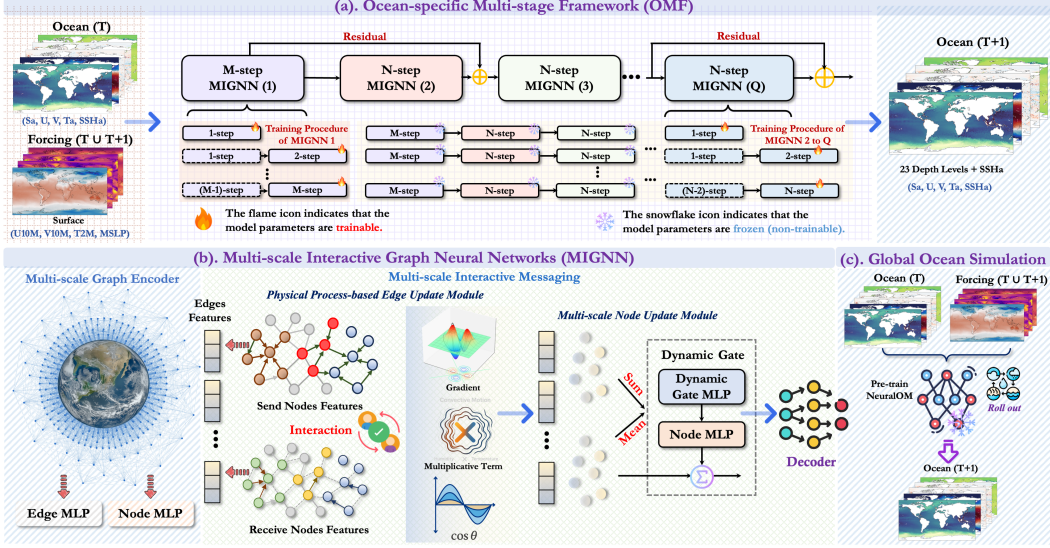


Figure 1: Overview of Our NeuralOM. (a) The overall architecture of the ocean-specific multi-stage framework, input variables (subtracting climatology for periodic variables), multi-model stage, and visualization of simulation ocean variables; (b) The proposed multi-scale interactive graph neural networks; (c) The global ocean simulation module uses a rollout approach to generate future results.

$\mathcal{E}^{\text{G2M}}$  and  $\mathcal{E}^{\text{M2G}}$  are the unidirectional edges that connect lat-lon grid nodes and mesh nodes. All scales share the same set of nodes  $\mathcal{V}$  but with multi-level edges. Then, we apply an MLP to map the data to the latent space, which can be defined as:

$$(\mathcal{V}_f^G, h, \mathcal{E}_f, \mathcal{E}_f^{\text{G2M}}, \mathcal{E}_f^{\text{M2G}}) = \text{MLP}(X_t, \mathcal{V}, \mathcal{E}_m, \mathcal{E}^{\text{G2M}}, \mathcal{E}^{\text{M2G}}), \quad (6)$$

$$\text{MLP} = \mathcal{N}(\sigma(\mathcal{L}(\cdot))), \quad (7)$$

where,  $\mathcal{L}(\cdot)$  is the linear function.  $\sigma(\cdot)$  is the SiLU activation function,  $\mathcal{N}(\cdot)$  is the LayerNorm function.  $X_t, \mathcal{V}, \mathcal{E}, \mathcal{E}^{\text{G2M}}$ , and  $\mathcal{E}^{\text{M2G}}$  are embedded features of grid nodes, mesh nodes, mesh edges, grid to mesh edges, and mesh to grid edges. Then, we update the grid2mesh edge features using information from the adjacent nodes:

$$\mathcal{E}_f^{\text{G2M}'} = \text{ESMLP}(\mathcal{V}_f^G, h, \mathcal{E}_f^{\text{G2M}}), \quad (8)$$

where,  $\text{ESMLP}(\cdot)$  is the Edge Sum MLP [27]. The mesh node features are updated by an MLP:

$$h' = \text{MLP}_{e1}(h, \sum \mathcal{E}_f^{\text{G2M}'}), \quad (9)$$

where,  $\sum \mathcal{E}_f^{\text{G2M}'}$  are the edges that arrives at mesh node. The grid node features are updated using another MLP:

$$\mathcal{V}_f^{G'} = \text{MLP}_{e2}(\mathcal{V}_f^G). \quad (10)$$

Finally, the residual connections are applied to update  $\mathcal{E}_f^{\text{G2M}}$ ,  $h$ , and  $\mathcal{V}_f^G$  again:

$$\mathcal{E}_f^{\text{G2M}} = \mathcal{E}_f^{\text{G2M}} + \mathcal{E}_f^{\text{G2M}'}, h = h + h', \mathcal{V}_f^G = \mathcal{V}_f^G + \mathcal{V}_f^{G'}. \quad (11)$$

### 3.2.2 Multi-scale Interactive Messaging

To make the message passing more consistent with the evolution process of the ocean dynamics system, we propose a module called Multi-scale Interactive Messaging (MIM). MIM includes a physical process-based edge update module and a multi-scale node update module. In our setup, 16 MIMs are applied to conduct messaging.

**Physical Process-based Edge Update Module.** In ocean simulation, ocean currents, temperature, salinity, and other factors interact with each other, and these interactions span different scales and layers. Unlike traditional MLP-based update strategy, which update edges by simply concatenating

edges and nodes, we introduce a physical process-based edge update module to more accurately simulate the dynamic relationships in the ocean system. For the sender node feature  $\mathbf{h}_{s(i)}$  and receiver nodes feature  $\mathbf{h}_{r(i)}$ , we first calculate their mutual interaction:

$$\mathbf{h}_{d(i)} = \mathbf{h}_{s(i)} - \mathbf{h}_{r(i)}, \quad (12)$$

where,  $\mathbf{h}_{d(i)}$  represents the variation in features between neighboring nodes, capturing the gradient changes of quantities such as flow velocity and salinity in the ocean. For example, when simulating changes in ocean currents, the velocity differences can indicate the energy transfer and dynamic characteristics of different ocean regions.

$$\mathbf{h}_{mp(i)} = \mathbf{h}_{s(i)} * \mathbf{h}_{r(i)}, \quad (13)$$

where,  $\mathbf{h}_{mp(i)}$  represents the multiplicative coupling relationship between nodes, similar to the coupling phenomenon between temperature and salinity in the ocean. The temperature and salinity of seawater together determine its density, which is crucial for modeling deep ocean currents.

$$\mathbf{h}_{cos(i)} = \cos(\mathbf{h}_{s(i)}, \mathbf{h}_{r(i)}), \quad (14)$$

where,  $\mathbf{h}_{cos(i)}$  is the cosine similarity between different nodes. For the ocean systems, it can be used to identify similar water masses or marine subsystems. For instance, when the changes in seawater temperature and salinity become consistent, it may indicate that these two ocean regions are influenced by similar climate systems, allowing information to be transmitted through similarity and improving the accuracy of the simulation. We define a function  $\mathcal{R}(\cdot)$  to fuse mesh node features and the features produced by the interaction:

$$\mathcal{R}(x) = \sigma(\mathcal{N}(\mathcal{L}(\mathcal{C}(x))))), \quad (15)$$

where,  $\mathcal{C}$  represents the concatenate function. Then, the fused mesh node features can be obtained by:

$$\mathbf{h}_{s(i)} = \mathcal{R}(\mathbf{h}_{s(i)}, \mathbf{h}_{mp(i)}, \mathbf{h}_{mp(i)}, \mathbf{h}_{cos(i)}), \mathbf{h}_{r(i)} = \mathcal{R}(\mathbf{h}_{r(i)}, \mathbf{h}_{mp(i)}, \mathbf{h}_{mp(i)}, \mathbf{h}_{cos(i)}). \quad (16)$$

Subsequently, the edge features are updated using the information from adjacent nodes:

$$\mathcal{E}'_f = \mathbf{W}_e \mathcal{E}_f, h'_s = \mathbf{W}_s h_s, h'_r = \mathbf{W}_r h_r + \mathbf{b}_r, \quad (17)$$

$$\mathbf{h}_{sum} = \mathcal{E}'_f + h'_s + h'_r, \quad (18)$$

$$\mathcal{E}'_f = \mathcal{N}(\mathbf{W} \cdot \sigma(h_{sum}) + \mathbf{b}), \quad (19)$$

where,  $\mathbf{W}_e$ ,  $\mathbf{W}_s$ ,  $\mathbf{W}_r$  are the linear transformation matrix of edge features, send node feature, and receive node features.  $\mathbf{W}$  is the linear transformation matrix of output layer.  $b_r$  and  $b$  are the bias. Finally, the edge features are updated using the residual connection:

$$\mathcal{E}_f = \mathcal{E}'_f + \mathcal{E}_f. \quad (20)$$

**Multi-scale Node Update Module.** Unlike traditional node update strategies, which typically sum or average the features of neighboring nodes, we consider the movements of the ocean at different scales. To achieve adaptive adjustment of aggregation methods across different scales, we introduce a multi-scale node update module that dynamically adjusts the weights of the aggregation strategy. For rapid local ocean dynamics with smaller scales, the gating mechanism automatically tends to favor sum aggregation, capturing the local rapid dynamic changes quickly and accurately. Conversely, when the model identifies that the motion scale around the node is larger and the changes are slower, it tends to prefer mean aggregation, which achieves a smoother and more robust representation of the large-scale ocean state.

Specifically, in the ocean system, meso- and small-scale movements (such as eddies, localized strong upwelling, coastal currents, etc.) exhibit distinct characteristics of localized energy concentration and rapid dynamic changes. In these scenarios, the influence of adjacent regions on a node is often cumulative, such as the concentrated propagation of local heat, momentum, or salt flux. In such cases, the sum aggregation strategy, by directly adding the contributions from surrounding nodes, more accurately reflects the rapid evolution and locally concentrated dynamic features, which can be expressed as:

$$h'_{sum} = \text{MLP}_{sum}(h, \sum \mathcal{E}'_f) \quad (21)$$

For large-scale, slowly varying ocean movements (such as the global ocean circulation, thermohaline circulation, and long-term ocean current trends), the differences between nodes and the extent of

local fluctuations are smaller, and information transfer between neighboring nodes tends to be in a relatively steady and averaged state. In this case, the mean aggregation strategy can more stably capture long-term trends and the overall balanced state, avoiding the over-influence of short-term local disturbances on the large-scale state, which can be expressed as:

$$h'_{mean} = \text{MLP}_{mean}(h, \sum \mathcal{E}'_f). \quad (22)$$

Then, we use  $h'_{sum}$  and  $h'_{mean}$  to calculate gating coefficient:

$$\gamma = \text{MLP}_g(\mathcal{C}(h'_{sum}, h'_{mean})). \quad (23)$$

Finally, an MLP and a residual connection are used to update the node features:

$$h' = \text{MLP}_{node}(\gamma \cdot h'_{sum} + (1 - \gamma) \cdot h'_{mean}). \quad (24)$$

### 3.2.3 Decoder

The role of the decoder is to decode the information from the latent space to the lat-lon grid. We first use the information from the adjacent nodes to update mesh2grid features:

$$\mathcal{E}_f^{\text{M2G}'} = \text{ESMLP}(\mathcal{V}_f^G, h, \mathcal{E}_f^{\text{M2G}}). \quad (25)$$

Then, we update the grid node features using the information of edges that arrive at the grid nodes:

$$\mathcal{V}_f^{G'} = \text{MLP}_{d1}(\mathcal{V}_f^G, \sum \mathcal{E}_f^{\text{M2G}'}), \quad (26)$$

Subsequently, we apply residual connection to update grid node features:

$$\mathcal{V}_f^G = \mathcal{V}_f^G + \mathcal{V}_f^{G'}. \quad (27)$$

Finally, we use an MLP to predict the next step results:

$$\hat{O}_{t+1} = \text{MLP}_{d2}(\mathcal{V}_f^G). \quad (28)$$

## 3.3 Optimization

We apply the relative  $L_2$  loss function to train each component of NeuralOM, which can be defined as:

$$\mathcal{L}_2 = \frac{1}{KHW} \sum_{k=1}^K \sum_{i=1}^H \sum_{j=1}^W \frac{(\hat{O}_{i,j,k}^{t+l\delta t} - O_{i,j,k}^{t+l\delta t})^2}{(O_{i,j,k}^{t+l\delta t})^2}, \quad (29)$$

where,  $\hat{O}_{i,j,k}^{t+l\delta t}$  and  $O_{i,j,k}^{t+l\delta t}$  are the predicted and ground truth for ocean variables (channels)  $k$  at spatial location  $(i, j)$  and time  $t + l\delta t$ ;  $K$  is the number of variables;  $H$  and  $W$  are the height and width of the spatial dimensions, respectively;  $\delta t$  is the time interval of single-step simulation (we use  $\delta t = 24$  hours).

## 3.4 Global Ocean Simulation

As illustrated in Figure 1(c), our inference procedure follows a rollout strategy: starting from the initial state  $\mathbf{X}_0$ , the trained model autoregressively feeds its own previous simulations together with the corresponding external forcing into the next time step. Previous studies have shown that evaluating an ocean model with forecast atmospheric fields can blur the distinctions among different ocean models, because errors in the atmospheric forecasts tend to dominate and “smooth out” their performance differences [38, 32]. In other words, when an ocean-only model is driven by biased forecast forcing, a well-designed ocean model can appear worse, while a poorer one can appear better. Consequently, a well-reliable assessment of an ocean model’s skill is obtained by using ground truth atmospheric forcing rather than forecast fields. Therefore, we use the ground truth atmospheric forcing to drive ocean models for comprehensive comparisons.

## 4 Experiment

In this section, we thoroughly evaluate the performance of NeuralOM, including metric results and visual results. We conduct all experiments on 64 NVIDIA A100 GPUs.

Table 1: In the global ocean simulation task, we compare the performance of our NeuralOM with 3 baselines. The average results for all 92 ocean variables of RMSE and ACC are recorded. Given the magnitude of the values for different variables, we report the normalized RMSE. A smaller RMSE ( $\downarrow$ ) and a bigger ACC ( $\uparrow$ ) indicate better performance. The best results are in **bold**, and the second best are with underline.

MODEL	METRIC							
	40-DAY		45-DAY		50-DAY		60-DAY	
	RMSE	ACC	RMSE	ACC	RMSE	ACC	RMSE	ACC
FOURCASTNET [26] <small>ARXIV 2022</small>	5.6336	0.0781	>10	0.0189	>10	0.0046	>10	0.0007
CIRT [21] <small>ICLR 2025</small>	2.7525	0.0143	2.8700	0.0115	2.9528	0.0099	3.0645	0.0081
WENHAI [5] <small>NATURE COMMUNICATIONS 2025</small>	<u>0.7200</u>	<u>0.5067</u>	<u>0.7468</u>	<u>0.4705</u>	<u>0.7702</u>	<u>0.4386</u>	<u>0.8093</u>	<u>0.3852</u>
NEURALOM (OURS)	<b>0.6619</b>	<b>0.5210</b>	<b>0.6785</b>	<b>0.4916</b>	<b>0.6926</b>	<b>0.4656</b>	<b>0.7158</b>	<b>0.4212</b>
NEURALOM (PROMOTION)	8.07%	2.84%	9.15%	4.49%	10.07%	6.16%	11.55%	9.33%

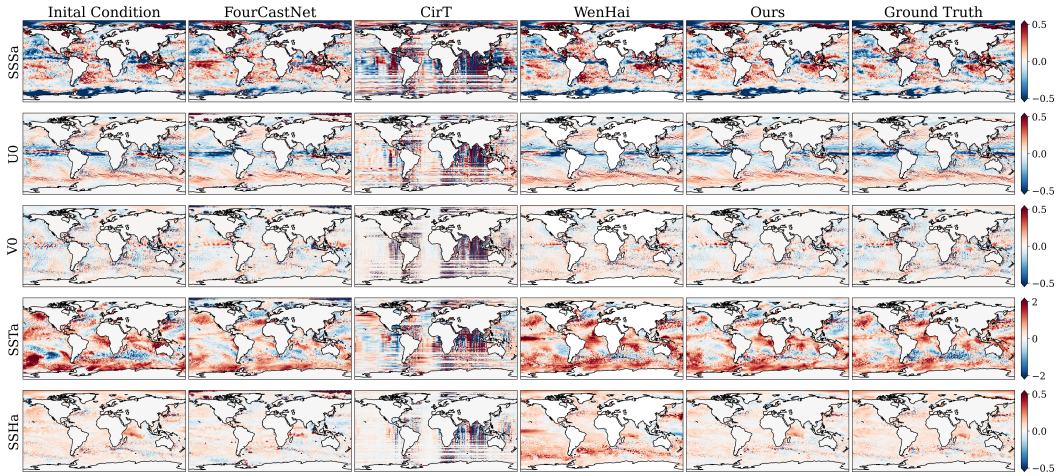


Figure 2: 60-day simulation results of different models.

#### 4.1 Benchmarks and Baselines

We conduct the experiments on GORYS12 reanalysis data, which offers daily mean data covering latitudes between  $-80^\circ$  and  $90^\circ$  spanning between 1993 and 2023. The subset we use includes years from 1993 to 2020, which is 1993-2017 for training, 2018-2019 for validating, and 2020 for testing. We use 4 depth level ocean variables (each with 23 depth levels, corresponding to 0.49 m, 2.65 m, 5.08 m, 7.93 m, 11.41 m, 15.81 m, 21.60 m, 29.44 m, 40.34 m, 55.76 m, 77.85 m, 92.32 m, 109.73 m, 130.67 m, 155.85 m, 186.13 m, 222.48 m, 266.04 m, 318.13 m, 380.21 m, 453.94 m, 541.09 m and 643.57 m), Sea salintiy (S), Sea stream zonal velocity (U), Sea stream meridonal velocity (V), Sea temperature (T), and 1 surface level variable Sea surface height (SSH). We downsampling them to  $1/2$  degree ( $H=361$ ,  $W=720$ ). And we use the data with size  $360 \times 720$ . 4 atmosphere variables are used as forcing. More details can be found in the Appendix. We compare the simulation performance of NeuralOM with 3 data-driven models (FourCastNet [26], CirT [21], and WenHai [5]). FourCastNet is an atmospheric backbone model with good performance. CirT is a SOTA subseasonal-to-seasonal atmosphere prediction model that is similar to our simulation time scale. WenHai is a SOTA ML-based ocean model that outperforms traditional numerical models and ML-based models. Specifically, we directly use the inference code released by WenHai’s author to produce the simulation results of WenHai. For other baselines and our NeuralOM, we retrain them in the same framework and settings.

#### 4.2 Evaluation Metrics

We utilize four metrics, RMSE (Root Mean Square Error), ACC (Anomalous Correlation Coefficient), CSI (Critical Success Index), and SEDI (Symmetric Extremal Dependence Index) to evaluate the

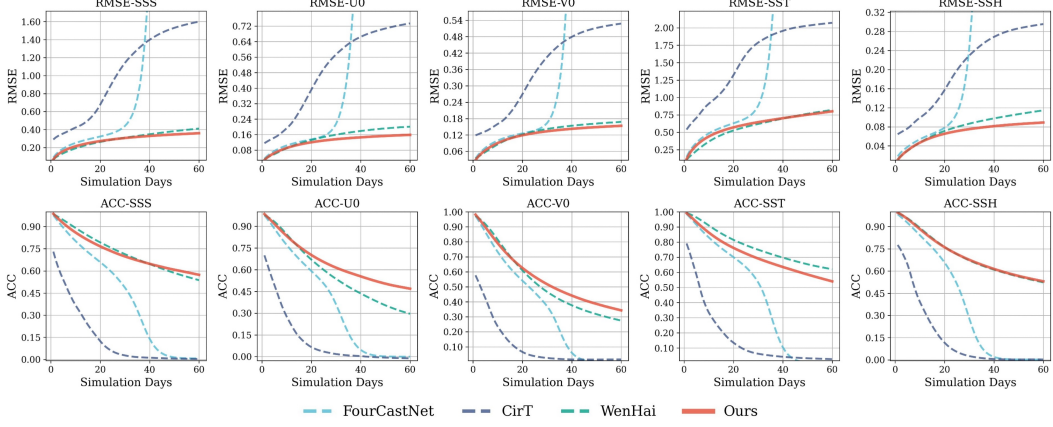


Figure 3: The latitude-weighted RMSE (lower is better) and ACC (higher is better) results of several important ocean surface variables.

Table 2: Ablation Studies on whether subtracting the climatology from periodicity variables will improve the simulation performance, the best results are in **bold**.

VARIANTS	23 LAYERS S		23 LAYERS T		SSH	
	RMSE	ACC	RMSE	ACC	RMSE	ACC
NEURALOM W/O SUBTRACT CLIMATOLOGY	0.0515	0.1061	0.1518	0.4535	0.2424	0.5747
NEURALOM W SUBTRACT CLIMATOLOGY	<b>0.0105</b>	<b>0.6412</b>	<b>0.0985</b>	<b>0.6508</b>	<b>0.1374</b>	<b>0.6695</b>

simulation performance, which can be defined as:

$$\text{RMSE}(\mathcal{J}, t) = \sqrt{\frac{\sum_{i=1}^{N_{\text{lat}}} \sum_{j=1}^{N_{\text{lon}}} L(i) \left( \hat{\mathbf{A}}_{ij,t}^{\mathcal{J}} - \mathbf{A}_{ij,t}^{\mathcal{J}} \right)^2}{N_{\text{lat}} \times N_{\text{lon}}}}, \quad (30)$$

$$\text{ACC}(\mathcal{J}, t) = \frac{\sum_{i=1}^{N_{\text{lat}}} \sum_{j=1}^{N_{\text{lon}}} L(i) \hat{\mathbf{A}}'_{ij,t}{}^{\mathcal{J}} \mathbf{A}'_{ij,t}{}^{\mathcal{J}}}{\sqrt{\sum_{i=1}^{N_{\text{lat}}} \sum_{j=1}^{N_{\text{lon}}} L(i) \left( \hat{\mathbf{A}}'_{ij,t}{}^{\mathcal{J}} \right)^2 \times \sum_{i=1}^{N_{\text{lat}}} \sum_{j=1}^{N_{\text{lon}}} L(i) \left( \mathbf{A}'_{ij,t}{}^{\mathcal{J}} \right)^2}}, \quad (31)$$

where  $\mathbf{A}_{i,j,t}^{\mathcal{K}}$  represents the value of variable  $\mathcal{J}$  at horizontal coordinate  $(i, j)$  and time  $t$ . Latitude-dependent weights are defined as  $L(i) = N_{\text{lat}} \times \frac{\cos \phi_i}{\sum_{i'=1}^{N_{\text{lat}}} \cos \phi_{i'}}$ , where  $\phi_i$  is the latitude at index  $i$ . The anomaly of  $A$ , denoted as  $A'$ , is computed as the deviation from its climatology, which corresponds to the long-term mean of the meteorological state estimated from multiple years of training data. RMSE and ACC are averaged across all time steps and spatial coordinates, providing summary statistics for each variable  $\mathcal{J}$  at a given lead time  $\Delta t$ .

$$\text{CSI}(\mathcal{J}, t) = \frac{\text{TP}}{\text{TP} + \text{FP} + \text{FN}}, \quad (32)$$

$$\text{SEDI}(\mathcal{J}, t) = \frac{\log(F) - \log(H) - \log(1 - F) + \log(1 - H)}{\log(F) + \log(H) + \log(1 - F) + \log(1 - H)}, \quad (33)$$

where, true positives (TP) represent the number of instances in which the ocean state is correctly simulated, while false positives (FP) and false negatives (FN) are defined analogously.  $F = \frac{\text{FP}}{\text{FP} + \text{TP}}$  is the false alarm rate, and  $H = \frac{\text{TP}}{\text{TP} + \text{FN}}$  represents the hit rate.

### 4.3 Global Ocean Simulation

Given the magnitude of the values for different variables, we report the normalized RMSE. We first normalize the 93 ocean variables and then calculate the indicators for the 240 initial conditions (ICs) starting from 1 Jan. 2020, and each IC will be updated one day later.

As shown in Table 1, NeuralOM achieves competitive performance compared with the state-of-the-art models. As shown in Figure 2, NeuralOM is closer to the ground truth. We also show the simulation results of several important surface variables in Figure 3, which are not normalized. It can be seen that state-of-the-art atmosphere prediction model, such as CirT, perform poorly in ocean scenes. A main reason may lays on the different nature of atmosphere and ocean dynamic systems. In contrast, our proposed NeuralOM performs satisfactorily in subseasonal-to-seasonal ocean simulation. This improvement is primarily attributed to integrating the proposed ocean-specific multi-stage framework and multi-scale interactive graph neural network, which effectively captures the ocean’s small change nature and accurately models the evolution of ocean dynamics at different time scales. More results at other depth-level layers can be found in the Appendix. It is worth noting that our NeuralOM achieves competitive results compared with the SOTA WenHai model training using 1/12 degree data, although we train NeuralOM using lower resolution data with 1/2 degree.

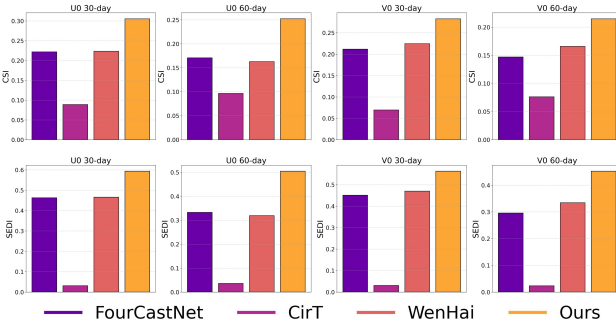


Figure 4: The CSI and SEDI results of extreme event assessment.

#### 4.4 Extreme Events Assessment

We apply CSI and SEDI to evaluate the simulation ability for extreme events. As shown in Figure 4, we calculate the CSI and SEDI results of U0 and V0 for 50 ICs. A bigger value means better performance to extreme event simulation. Our proposed NeuralOM achieves competitive performance.

#### 4.5 Ablation Studies

To assess the effectiveness of the proposed method, we conduct detailed ablation studies, as summarized in Table 2 and Table 3. Specially, we introduce several model variants: (1) **NeuralOM W/O Subtract Climatology**, we don’t subtract climatology for periodicity variables before input them to the model. (2) **NeuralOM w Subtract Climatology**, we subtract the climatology for the periodicity variables. (3) **NeuralOM w/o OMF**, we remove ocean-specific multi-stage framework. (4) **NeuralOM w/o PEM**, we remove physical process-based edge update module. (5) **NeuralOM w/o MNM Sum**, we remove the sum aggregation strategy in the multi-scale node update module. (6) **NeuralOM w/o MNM Mean**, we remove the mean aggregation strategy in the multi-scale node update module. (7) **NeuralOM**, the full version of NeuralOM. The above metrics are based on 30-day simulation results (50ICs for (1),(2), and 100ICs for others). Experimental results show that removing any single component impairs NeuralOM’s performance, thereby validating the effectiveness of our proposed method.

Table 3: Ablation Studies on model design, the best results are in **bold**.

Variants	RMSE	ACC
NeuralOM w/o OMF	0.6692	0.5503
NeuralOM w/o PEM	0.6865	0.5168
NeuralOM w/o MNM Sum	0.7037	0.5361
NeuralOM w/o MNM Mean	0.6978	0.5161
<b>NeuralOM</b>	<b>0.6097</b>	<b>0.5983</b>

## 5 Conclusion

This work presents NeuralOM, a neural ocean foundation model tailored for Subseasonal-to-Seasonal (S2S) simulation. Our proposed ocean-specific multi-stage framework ensures accurate modeling of the ocean’s slow dynamics, while the multi-scale interactive messaging module enables the representation of intricate dynamical interactions, which accurately model the evolution process of ocean dynamics at the S2S time scale. Extensive experimental results demonstrate that NeuralOM significantly outperforms existing state-of-the-art models in both S2S and extreme event simulation, confirming its potential to revolutionize ocean and climate simulation tasks.

## Acknowledgements

This work was supported by the National Natural Science Foundation of China (42125503, 42430602).

## References

- [1] Kaifeng Bi, Lingxi Xie, Hengheng Zhang, Xin Chen, Xiaotao Gu, and Qi Tian. Accurate medium-range global weather forecasting with 3d neural networks. *Nature*, 619(7970):533–538, 2023.
- [2] Xiaona Chang, Jianchao Wang, Guanjun Zhang, Ming Yang, Yanfeng Xi, Chenghang Xi, Gang Chen, Xiu Nie, Bin Meng, and Xueping Quan. Predicting colorectal cancer microsatellite instability with a self-attention-enabled convolutional neural network. *Cell Reports Medicine*, 4(2), 2023.
- [3] Yipeng Chen, Yishuai Jin, Zhengyu Liu, Xingchen Shen, Xianyao Chen, Xiaopei Lin, Rong-Hua Zhang, Jing-Jia Luo, Wenjun Zhang, Wansuo Duan, et al. Combined dynamical-deep learning enso forecasts. *Nature Communications*, 16(1):3845, 2025.
- [4] Nathaniel Cresswell-Clay, Bowen Liu, Dale Durran, Andy Liu, Zachary I Espinosa, Raul Moreno, and Matthias Karlbauer. A deep learning earth system model for stable and efficient simulation of the current climate. *arXiv preprint arXiv:2409.16247*, 2024.
- [5] Yingzhe Cui, Ruohan Wu, Xiang Zhang, Ziqi Zhu, Bo Liu, Jun Shi, Junshi Chen, Hailong Liu, Shenghui Zhou, Liang Su, et al. Forecasting the eddy ocean with a deep neural network. *Nature Communications*, 16(1):2268, 2025.
- [6] Antoine Delaunay and Hannah M Christensen. Interpretable deep learning for probabilistic mjo prediction. *Geophysical Research Letters*, 49(16):e2022GL098566, 2022.
- [7] Tobias Sebastian Finn, Charlotte Durand, Alban Farchi, Marc Bocquet, Pierre Rampal, and Alberto Carrassi. Generative diffusion for regional surrogate models from sea-ice simulations. *Journal of Advances in Modeling Earth Systems*, 16(10):e2024MS004395, 2024.
- [8] PA Francis, AK Jithin, JB Effy, Abhisek Chatterjee, Kunal Chakraborty, A Paul, B Balaji, SSC Sheno, P Biswamoy, Arnab Mukherjee, et al. High-resolution operational ocean forecast and reanalysis system for the indian ocean. *Bulletin of the American Meteorological Society*, 101(8):E1340–E1356, 2020.
- [9] Yuan Gao, Hao Wu, Ruiqi Shu, Huanshuo Dong, Fan Xu, Rui Chen, Yiibo Yan, Qingsong Wen, Xuming Hu, Kun Wang, et al. Oneforecast: A universal framework for global and regional weather forecasting. In *International Conference on Machine Learning*. PMLR, 2025.
- [10] Zijie Guo, Pumeng Lyu, Fenghua Ling, Lei Bai, Jing-Jia Luo, Niklas Boers, Toshio Yamagata, Takeshi Izumo, Sophie Cravatte, Antonietta Capotondi, et al. Data-driven global ocean modeling for seasonal to decadal prediction. *arXiv preprint arXiv:2405.15412*, 2024.
- [11] Yoo-Geun Ham, Jeong-Hwan Kim, and Jing-Jia Luo. Deep learning for multi-year enso forecasts. *Nature*, 573(7775):568–572, 2019.
- [12] Rixu Hao, Yuxin Zhao, Shaoqing Zhang, and Xiong Deng. Deep learning for ocean forecasting: A comprehensive review of methods, applications, and datasets. *IEEE Transactions on Cybernetics*, 2025.
- [13] Kaiming He, Xinlei Chen, Saining Xie, Yanghao Li, Piotr Dollár, and Ross Girshick. Masked autoencoders are scalable vision learners. In *Proceedings of the IEEE/CVF conference on computer vision and pattern recognition*, pages 16000–16009, 2022.
- [14] Jie Hu, Bin Weng, Tianqiang Huang, Jianyun Gao, Feng Ye, and Lijun You. Deep residual convolutional neural network combining dropout and transfer learning for enso forecasting. *Geophysical Research Letters*, 48(24):e2021GL093531, 2021.

- [15] Michael G Jacox, Michael A Alexander, Dillon Amaya, Emily Becker, Steven J Bograd, Stephanie Brodie, Elliott L Hazen, Mercedes Pozo Buil, and Desiree Tommasi. Global seasonal forecasts of marine heatwaves. *Nature*, 604(7906):486–490, 2022.
- [16] Ham Kim, YG Ham, YS Joo, and SW Son. Deep learning for bias correction of mjo prediction. *Nature Communications*, 12(1):3087, 2021.
- [17] Remi Lam, Alvaro Sanchez-Gonzalez, Matthew Willson, Peter Wyrnsberger, Meire Fortunato, Ferran Alet, Suman Ravuri, Timo Ewalds, Zach Eaton-Rosen, Weihua Hu, et al. Learning skillful medium-range global weather forecasting. *Science*, 382(6677):1416–1421, 2023.
- [18] Chaehyeong Lee, Hajoong Song, Yeonju Choi, Ajin Cho, and John Marshall. Observed multi-decadal increase in the surface ocean’s thermal inertia. *Nature Climate Change*, pages 1–7, 2025.
- [19] Jingjing Liu, Baogang Jin, Lei Wang, and Lingyu Xu. Sea surface height prediction with deep learning based on attention mechanism. *IEEE Geoscience and Remote Sensing Letters*, 19:1–5, 2020.
- [20] Qi Liu and Jianwei Ma. Foundation models for geophysics: Review and perspective. *arXiv preprint arXiv:2406.03163*, 2024.
- [21] Yang Liu, Zinan Zheng, Jiashun Cheng, Fugee Tsung, Deli Zhao, Yu Rong, and Jia Li. Cirt: Global subseasonal-to-seasonal forecasting with geometry-inspired transformer. In *The Thirteenth International Conference on Learning Representations*, 2025.
- [22] Ze Liu, Yutong Lin, Yue Cao, Han Hu, Yixuan Wei, Zheng Zhang, Stephen Lin, and Baining Guo. Swin transformer: Hierarchical vision transformer using shifted windows. In *Proceedings of the IEEE/CVF international conference on computer vision*, pages 10012–10022, 2021.
- [23] Pumeng Lyu, Tao Tang, Fenghua Ling, Jing-Jia Luo, Niklas Boers, Wanli Ouyang, and Lei Bai. Resonet: Robust and explainable enso forecasts with hybrid convolution and transformer networks. *Advances in Atmospheric Sciences*, 41(7):1289–1298, 2024.
- [24] Rambod Mojjani, Ashesh Chattopadhyay, and Pedram Hassanzadeh. Interpretable structural model error discovery from sparse assimilation increments using spectral bias-reduced neural networks: A quasi-geostrophic turbulence test case. *Journal of Advances in Modeling Earth Systems*, 16(3):e2023MS004033, 2024.
- [25] Antonios Parasyris, Vassiliki Metheniti, Nikolaos Kampanis, and Sofia Darmaraki. Marine heatwaves in the mediterranean sea: A convolutional neural network study for extreme event prediction. *Ocean Science*, 21(3):897–912, 2025.
- [26] Jaideep Pathak, Shashank Subramanian, Peter Harrington, Sanjeev Raja, Ashesh Chattopadhyay, Morteza Mardani, Thorsten Kurth, David Hall, Zongyi Li, Kamyar Azizzadenesheli, et al. Fourcastnet: A global data-driven high-resolution weather model using adaptive fourier neural operators. *arXiv preprint arXiv:2202.11214*, 2022.
- [27] Tobias Pfaff, Meire Fortunato, Alvaro Sanchez-Gonzalez, and Peter Battaglia. Learning mesh-based simulation with graph networks. In *International conference on learning representations*, 2020.
- [28] Benyun Shi, Liu Feng, Hailun He, Yingjian Hao, Yue Peng, Miao Liu, Yang Liu, and Jiming Liu. A physics-guided attention-based neural network for sea surface temperature prediction. *IEEE Transactions on Geoscience and Remote Sensing*, 2024.
- [29] Zhensheng Shi, Haiyong Zheng, and Junyu Dong. Oceanvp: A hycom based benchmark dataset and a relational spatiotemporal predictive network for oceanic variable prediction. *Ocean Engineering*, 304:117748, 2024.
- [30] Na-Yeon Shin, Daehyun Kang, Daehyun Kim, June-Yi Lee, and Jong-Seong Kug. Data-driven investigation on the boreal summer mjo predictability. *npj Climate and Atmospheric Science*, 7(1):248, 2024.

- [31] Na-Yeon Shin, Daehyun Kim, Daehyun Kang, Hyemi Kim, and Jong-Seong Kug. Deep learning reveals moisture as the primary predictability source of mjo. *npj Climate and Atmospheric Science*, 7(1):11, 2024.
- [32] Ruiqi Shu, Hao Wu, Yuan Gao, Fanghua Xu, Ruijian Gou, Wei Xiong, and Xiaomeng Huang. Advanced forecasts of global extreme marine heatwaves through a physics-guided data-driven approach. *Environmental Research Letters*, 20(4):044030, 2025.
- [33] Tao Song, Jingyu Jiang, Wei Li, and Danya Xu. A deep learning method with merged lstm neural networks for ssha prediction. *IEEE Journal of Selected Topics in Applied Earth Observations and Remote Sensing*, 13:2853–2860, 2020.
- [34] Adam Subel and Laure Zanna. Building ocean climate emulators. *arXiv preprint arXiv:2402.04342*, 2024.
- [35] Aneesh C Subramanian, Magdalena A Balmaseda, Luca Centurioni, Rajib Chattopadhyay, Bruce D Cornuelle, Charlotte DeMott, Maria Flatau, Yosuke Fujii, Donata Giglio, Sarah T Gille, et al. Ocean observations to improve our understanding, modeling, and forecasting of subseasonal-to-seasonal variability. *Frontiers in Marine Science*, 6:427, 2019.
- [36] Di Sun, Zhao Jing, and Hailong Liu. Deep learning improves sub-seasonal marine heatwave forecast. *Environmental Research Letters*, 19(6):064035, 2024.
- [37] Nathaniel Trask, Amelia Henriksen, Carianne Martinez, and Eric Cyr. Hierarchical partition of unity networks: fast multilevel training. In *Mathematical and Scientific Machine Learning*, pages 271–286. PMLR, 2022.
- [38] Xiang Wang, Renzhi Wang, Ningzi Hu, Pinqiang Wang, Peng Huo, Guihua Wang, Huizan Wang, Senzhang Wang, Junxing Zhu, Jianbo Xu, et al. Xihe: A data-driven model for global ocean eddy-resolving forecasting. *arXiv preprint arXiv:2402.02995*, 2024.
- [39] Hao Wu, Kangyu Weng, Shuyi Zhou, Xiaomeng Huang, and Wei Xiong. Neural manifold operators for learning the evolution of physical dynamics. In *Proceedings of the 30th ACM SIGKDD Conference on Knowledge Discovery and Data Mining*, pages 3356–3366, 2024.
- [40] Wei Xiong, Yanfei Xiang, Hao Wu, Shuyi Zhou, Yuze Sun, Muyuan Ma, and Xiaomeng Huang. Ai-goms: Large ai-driven global ocean modeling system. *arXiv preprint arXiv:2308.03152*, 2023.
- [41] Nan Yang, Chong Wang, Meihua Zhao, Zimeng Zhao, Huiling Zheng, Bin Zhang, Jianing Wang, and Xiaofeng Li. Langya: Revolutionizing cross-spatiotemporal ocean forecasting. *arXiv preprint arXiv:2412.18097*, 2024.
- [42] Young-Min Yang, Jeong-Hwan Kim, Jae-Heung Park, Yoo-Geun Ham, Soon-Il An, June-Yi Lee, and Bin Wang. Exploring dominant processes for multi-month predictability of western pacific precipitation using deep learning. *Npj Climate and Atmospheric Science*, 6(1):157, 2023.

## A Data Details

### A.1 Dataset

We conduct the experiments on GORYS12 reanalysis data, offering daily mean data covering latitudes between  $-80^\circ$  and  $90^\circ$  spanning between 1993 and 2023, which can be downloaded from [https://data.marine.copernicus.eu/product/GLOBAL\\_MULTIYEAR\\_PHY\\_001\\_030/description](https://data.marine.copernicus.eu/product/GLOBAL_MULTIYEAR_PHY_001_030/description). The subset we use includes years from 1993 to 2020, which is 1993-2017 for training, 2018-2019 for validating, and 2020 for testing. We use 4 depth level ocean variables (each with 23 depth levels, corresponding to 0.49 m, 2.65 m, 5.08 m, 7.93 m, 11.41 m, 15.81 m, 21.60 m, 29.44 m, 40.34 m, 55.76 m, 77.85 m, 92.32 m, 109.73 m, 130.67 m, 155.85 m, 186.13 m, 222.48 m, 266.04 m, 318.13 m, 380.21 m, 453.94 m, 541.09 m and 643.57 m), Sea salinity (S), Sea stream zonal velocity (U), Sea stream meridional velocity (V), Sea temperature (T), and 1 surface level variable Sea surface height (SSH). To improve computational efficiency, we use bilinear interpolation to downsampling them to 1/2 degree ( $H=361$ ,  $W=720$ ). And to better adapt to the input of different architecture models, we use the data with size  $360 \times 720$ . 4 atmosphere variables from ERA5 are used as forcing, which include 10 metre u wind component (U10M), 10 metre v wind component (V10M), 2 metre temperature (T2M), and mean sea level pressure (MSLP). The ERA5 data can be downloaded from <https://cds.climate.copernicus.eu/>, the official website of Climate Data Store (CDS). All the data we used are shown in Table 4.

### A.2 Data preprocessing

Different ocean and forcing variables exhibit substantial variations in magnitude. To enable the model to concentrate on accurate simulation rather than learning the inherent magnitude discrepancies among variables, we normalize the input data prior to model ingestion. Specifically, for ocean variables, we compute the mean and standard deviation from the training dataset spanning the years 1993 to 2017. For forcing variables, we calculate these statistics from an extended dataset covering the period 1959 to 2017. Each variable thus possesses a dedicated mean and standard deviation. Before inputting data into the model, we normalize the data by subtracting the corresponding mean and dividing the respective standard deviation. For the ‘nan’ values of land, we fill them with zero before inputting the data into the model.

Table 4: The data details in this work.

Type	Full name	Abbreviation	Layers	Time	Dt	Spatial Resolution
Atmosphere	10 metre u wind component	U10M	1	1993-2020	24h	$0.5^\circ$
Atmosphere	10 metre v wind component	V10M	1	1993-2020	24h	$0.5^\circ$
Atmosphere	2 metre temperature	T2M	1	1993-2020	24h	$0.5^\circ$
Atmosphere	Mean sea level pressure	MSLP	1	1993-2020	24h	$0.5^\circ$
Ocean	Sea salinity	S	23	1993-2020	24h	$0.5^\circ$
Ocean	Sea stream zonal velocity	U	23	1993-2020	24h	$0.5^\circ$
Ocean	Sea stream meridional velocity	V	23	1993-2020	24h	$0.5^\circ$
Ocean	Sea temperature	T	23	1993-2020	24h	$0.5^\circ$
Ocean	Sea surface height	SSH	1	1993-2020	24h	$0.5^\circ$
Static	Land-sea mask	LSM	—	—	—	$0.5^\circ$

## B Algorithm

We summarize the overall framework of the ocean-specific multi-stage framework (OMF) in Algorithm 1 and multi-scale interactive graph neural networks (MIGNN) in Algorithm 2.

## C Model Training

For the ocean-specific multi-stage framework, we apply Q sub-models to progressively capture subtle changes in ocean variables. We train the first sub-model with M steps finetune. For other sub-models, we train them with N steps finetune. In our experiment, we set  $Q=2$ ,  $M=6$ , and  $N=10$  as an example.

---

**Algorithm 1** Ocean-specific Multi-stage Framework (OMF)

---

**Require:** Initial input data  $X_t$ .

**Ensure:** Next step ocean state  $O_{t+1}$ .

- 1: Initialize OMF
  - 2: **repeat**
  - 3:   **MIGNN (1)**
  - 4:   Apply the first MIGNN model to encode the combined input  $X_t = [O_t, F_t, F_{t+1}]$  into the intermediate results of the next step ocean state  $\hat{O}_{t+1}^1 = \mathcal{F}_1^M(X_t)$ .
  - 5:   **MIGNN (2)**
  - 6:   Apply the second MIGNN model to map  $\hat{O}_{t+1}^1$  into the intermediate results:  $\hat{O}_{t+1}^2 = \mathcal{F}_2^N(\hat{O}_{t+1}^1) + \hat{O}_{t+1}^1$ .
  - 7:   **MIGNN (Q)**
  - 8:   Apply the Q-th MIGNN model to map  $\hat{O}_{t+1}^{Q-1}$  into the final results:  $O_{t+1} = \mathcal{F}_Q^N(\hat{O}_{t+1}^{Q-1}) + \hat{O}_{t+1}^{Q-1}$ .
  - 9: **until** converged
  - 10: **return** OMF
- 

---

**Algorithm 2** Multi-scale Interactive Graph Neural Networks (MIGNN)

---

**Require:** Initial input data  $X_t$ .

**Ensure:** Next step ocean state  $O_{t+1}$ .

- 1: Initialize MIGNN
  - 2: **repeat**
  - 3:   **Encoder**
  - 4:   Embedding features of grid nodes  $X_t$ , mesh nodes  $\mathcal{V}$ , mesh edges  $\mathcal{E}_m$ , grid to mesh edges  $\mathcal{E}^{\text{G2M}}$ , and mesh to grid edges  $\mathcal{E}^{\text{M2G}}$  into latent space using separate MLP:  $(\mathcal{V}_f^G, h, \mathcal{E}_f, \mathcal{E}_f^{\text{G2M}}, \mathcal{E}_f^{\text{M2G}}) = \text{MLPs}(X_t, \mathcal{V}, \mathcal{E}_m, \mathcal{E}^{\text{G2M}}, \mathcal{E}^{\text{M2G}})$
  - 5:   Project the ocean state from the lat-lon grid into the mesh nodes:  $\mathcal{E}_f^{\text{G2M}'} = \text{ESMLP}(\mathcal{V}_f^G, h, \mathcal{E}_f^{\text{G2M}}), h' = \text{MLP}_{e1}(h, \sum \mathcal{E}_f^{\text{G2M}'})$
  - 6:   Update grid node feature:  $\mathcal{V}_f^{G'} = \text{MLP}_{e2}(\mathcal{V}_f^G)$
  - 7:   Apply residual connection to update the feature of grid to mesh edge, mesh node, and grid node again:  $\mathcal{E}_f^{\text{G2M}} = \mathcal{E}_f^{\text{G2M}} + \mathcal{E}_f^{\text{G2M}'}, h' = h + h', \mathcal{V}_f^G = \mathcal{V}_f^G + \mathcal{V}_f^{G'}$
  - 8:   **Multi-scale Interactive Massaging (MIM)**
  - 9:   Apply physical process-based edge update module (PEM) to update edge feature:  $\mathcal{E}_f' = \text{PEM}(\mathcal{E}_f, h_s, h_r)$
  - 10:   Apply multi-scale node update module (MNM) to update mesh node feature:  $h' = \text{MNM}(h, \sum \mathcal{E}_f')$
  - 11:   Apply residual connection to update the feature of edge and mesh node:  $\mathcal{E}_f = \mathcal{E}_f + \mathcal{E}_f', h = h + h'$
  - 12:   **Decoder** Project the feature from mesh back to lat-lon grid:  $\mathcal{E}_f^{\text{M2G}'} = \text{ESMLP}(\mathcal{V}_f^G, \mathcal{E}_f, \mathcal{E}_f^{\text{M2G}}), \mathcal{V}_f^{G'} = \text{MLP}_{d1}(\mathcal{V}_f^G, \sum \mathcal{E}_f^{\text{M2G}'}), \mathcal{V}_f^G = \mathcal{V}_f^G + \mathcal{V}_f^{G'}, O_{t+1} = \text{MLP}_{d2}(\mathcal{V}_f^G)$
  - 13: **until** converged
  - 14: **return** MIGNN
- 

Specifically, we train the first sub-model, denoted as  $\mathcal{F}_1^1$  with 200 epochs using 1-step supervision. The learning rate is set to 1e-3. And we use the cosine annealing scheduler to adjust the learning rate until the model converges. After that, we finetune  $\mathcal{F}_1^1$  with 10 epochs using 2-step supervision to get  $\mathcal{F}_1^2$ . Then, we finetune  $\mathcal{F}_1^2$  with 10 epochs using 3-step supervision to get  $\mathcal{F}_1^3$ . The learning rate is set to 1e-6. And we use the cosine annealing scheduler to adjust the learning rate until the model converges. The model  $\mathcal{F}_1^4, \mathcal{F}_1^5$ , and  $\mathcal{F}_1^M$  are finetuned same as  $\mathcal{F}_1^3$ . Then we freeze the parameters of  $\mathcal{F}_1^M$  and train the second sub-model  $\mathcal{F}_2^1$  with 200 epochs. The learning rate is set to 1e-6. And we use the cosine annealing scheduler to adjust the learning rate until the model converges. In practice, the model converges after a few epochs, and we stop the training early. The the  $\mathcal{F}_2^N$  can be get step

by step with same training produce as  $\mathcal{F}_2^1$ . Furthermore, the Q-th model  $\mathcal{F}_Q^N$  can be trained step by step if a higher accuracy is required. We train all baseline models and our NeuralOM using the same training framework. We will open-source all of our materials—including all training codes, detailed training procedures, testing codes, pre-trained weights, training logs, and more.

## D Additional Results

Additional quantitative results (RMSE and ACC across depth levels 109.73 m, 222.48 m, and 453.94 m) are shown in Figure 5. The RMSE and ACC represent the average performance for 240 ICs, starting from Jan. 1, 2020, and the interval of each IC is 1 day. Additional visual results are presented in Figure 6, Figure 7, Figure 8, Figure 9, Figure 10, and Figure 11, covering 17 important ocean variables across simulation time from 10 to 60 days, with the initial condition at Jun. 1, 2020. Specifically, for variables S, T, and SSH, where variations are subtle relative to their baseline values, anomalies are presented to highlight these minor but significant changes. Conversely, the original data are directly displayed for U and V. For clarity, examples of variable naming conventions are as follows: SSSa denotes sea surface salinity anomaly, Sa109 denotes salinity anomaly at 109.73 m, Sa222 denotes salinity anomaly at 222.48 m, and Sa453 denotes salinity anomaly at 453.94 m. U0 denotes the sea surface stream zonal velocity, U109 denotes the sea stream zonal velocity at 109.73 m, U222 denotes the sea stream zonal velocity at 222.48 m, and U453 denotes the sea stream zonal velocity at 453.94 m. Collectively, these supplementary results further demonstrate the efficacy of the proposed NeuralOM.

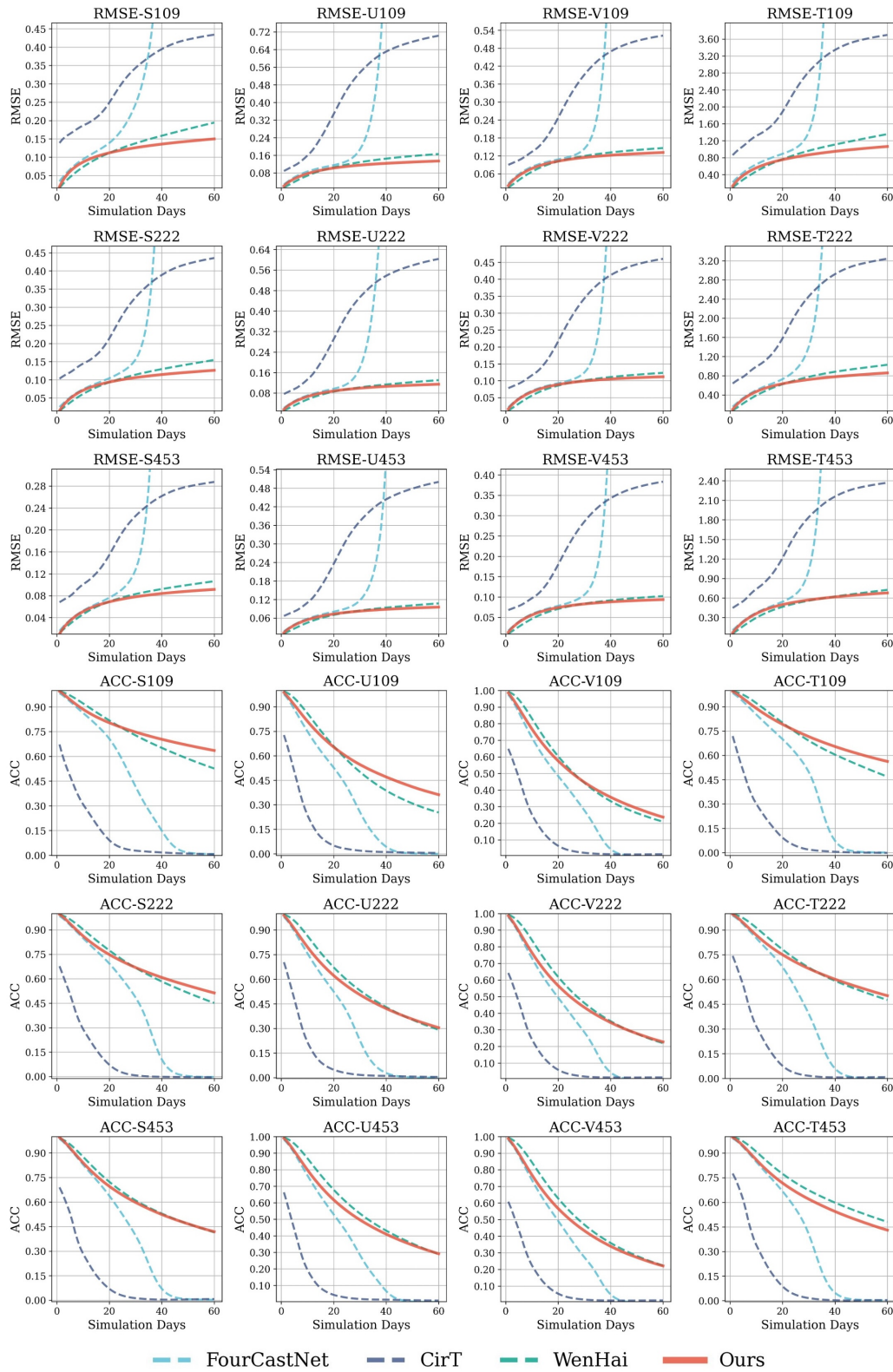


Figure 5: The latitude-weighted RMSE (lower is better) and ACC (higher is better) results of several important ocean variables (depth levels at 109.73 m, 222.48 m, and 453.94 m).

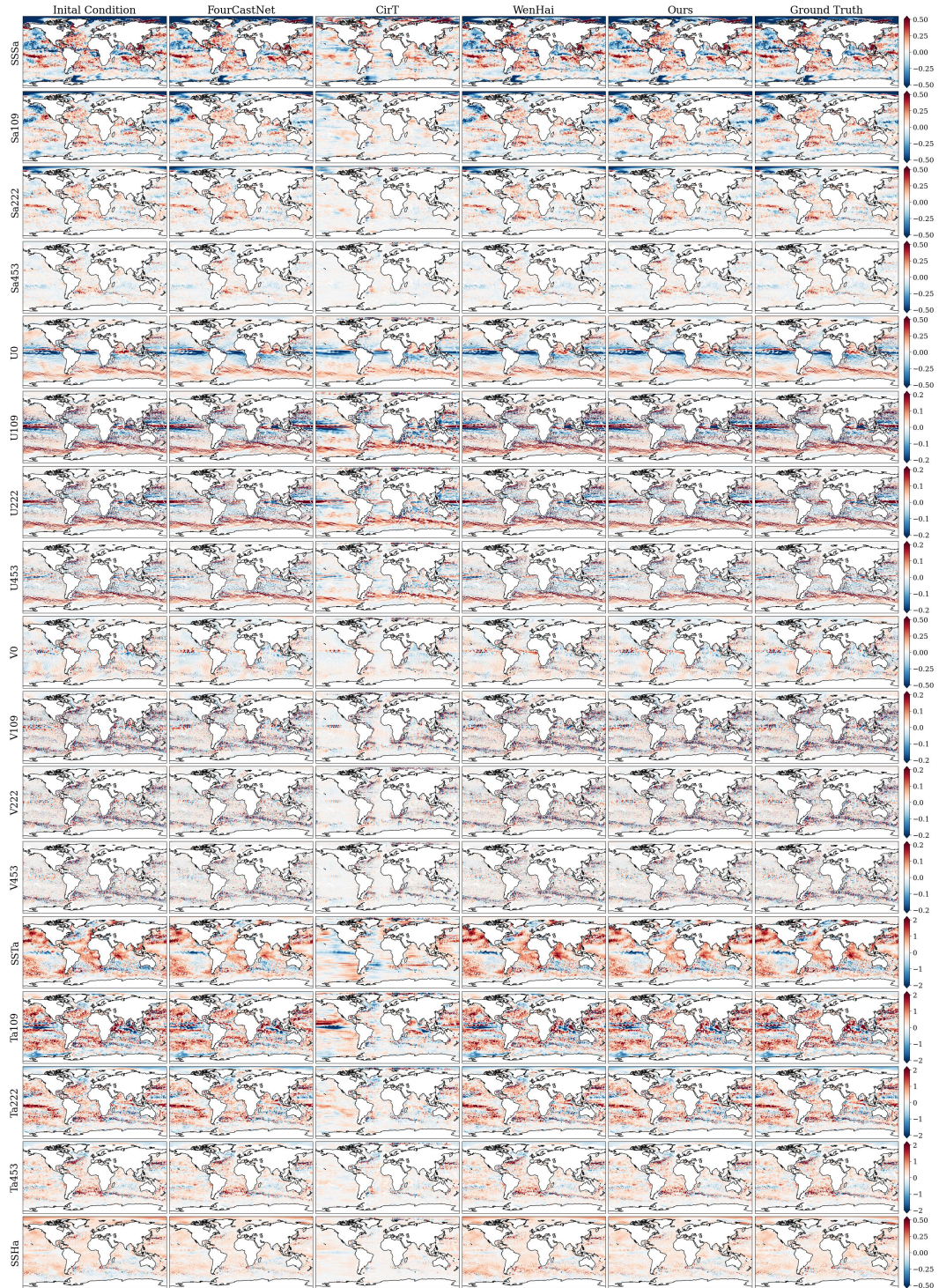


Figure 6: 10-day simulation results of different models.

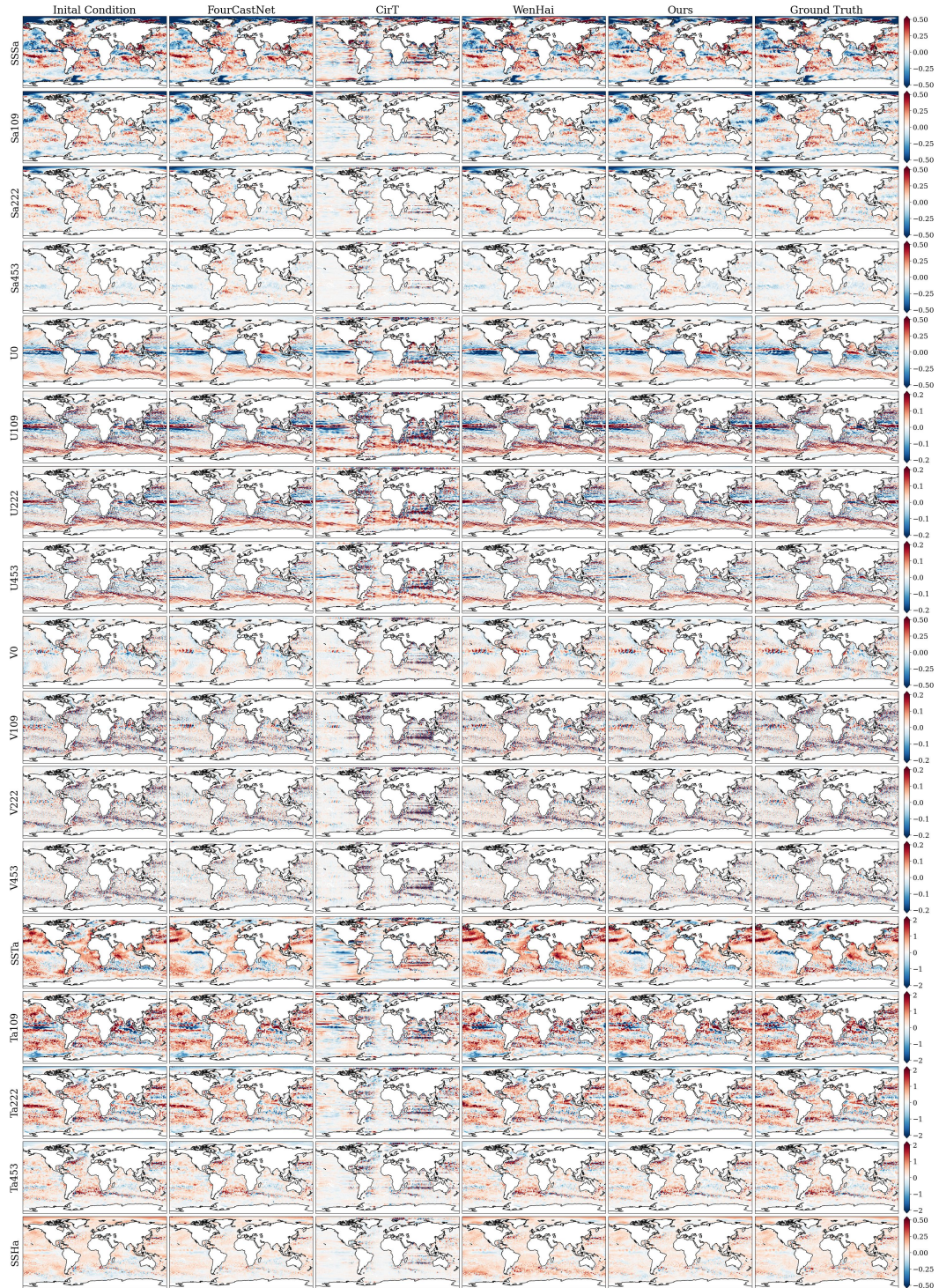


Figure 7: 20-day simulation results of different models.

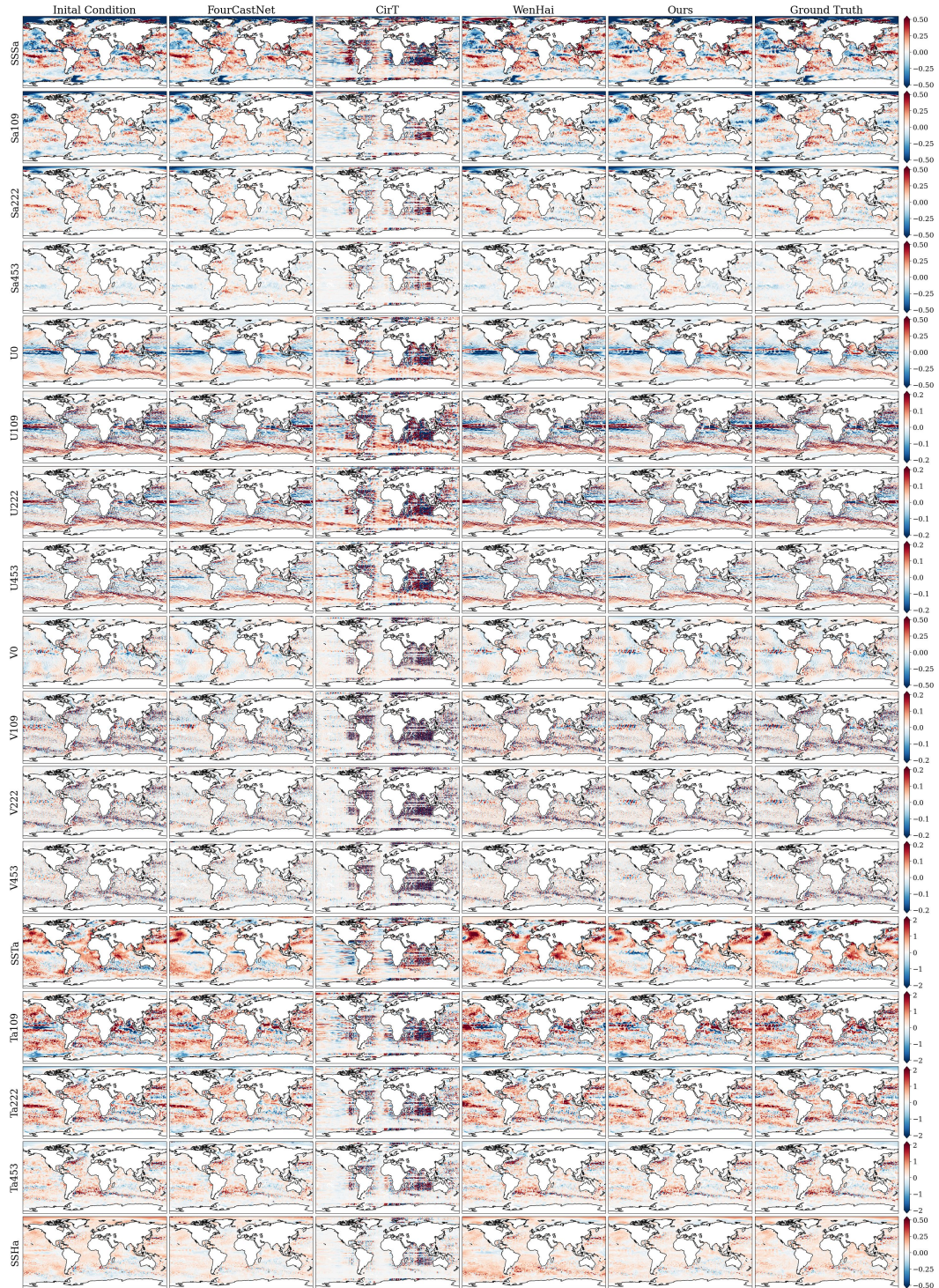


Figure 8: 30-day simulation results of different models.

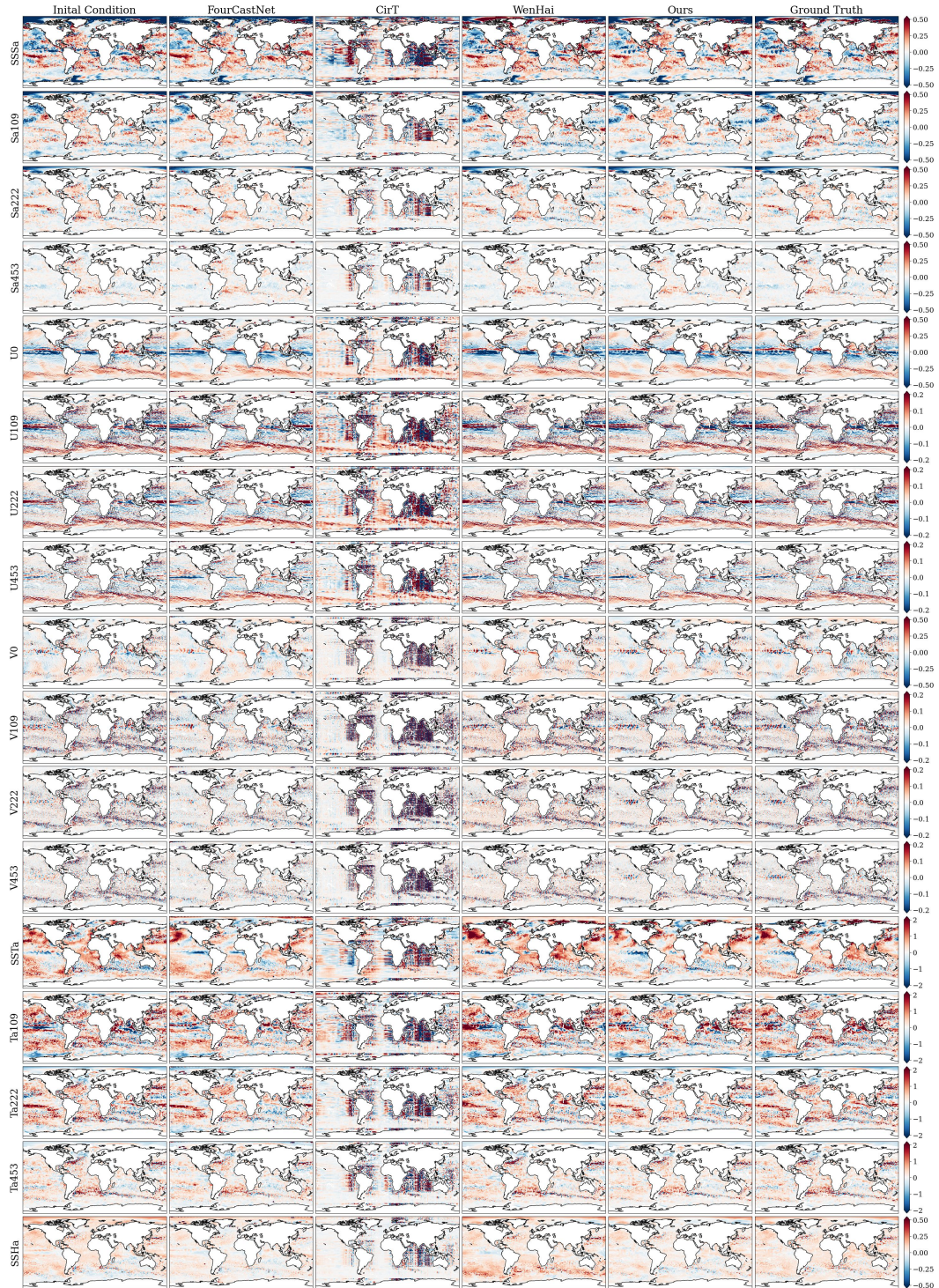


Figure 9: 40-day simulation results of different models.

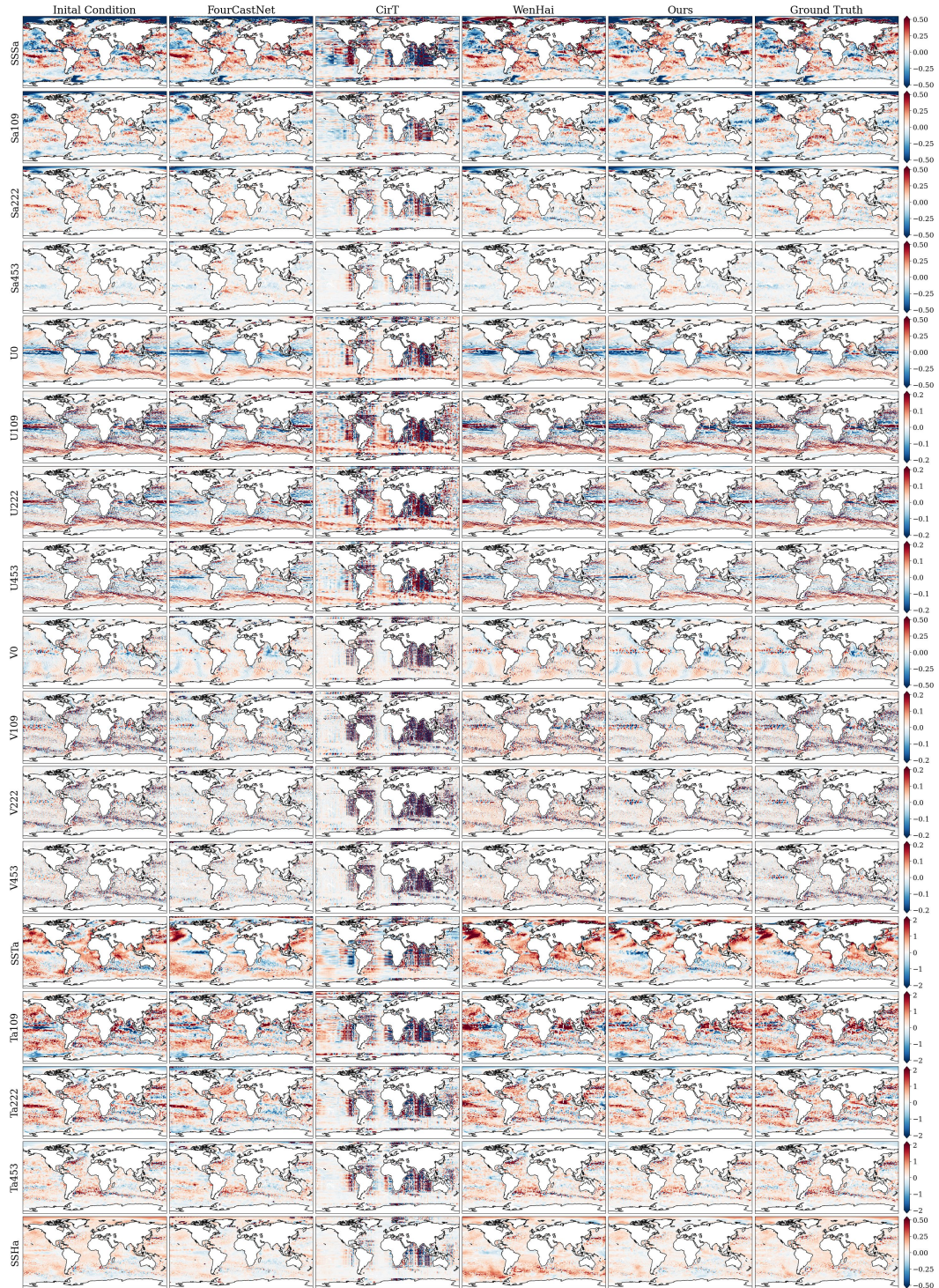


Figure 10: 50-day simulation results of different models.

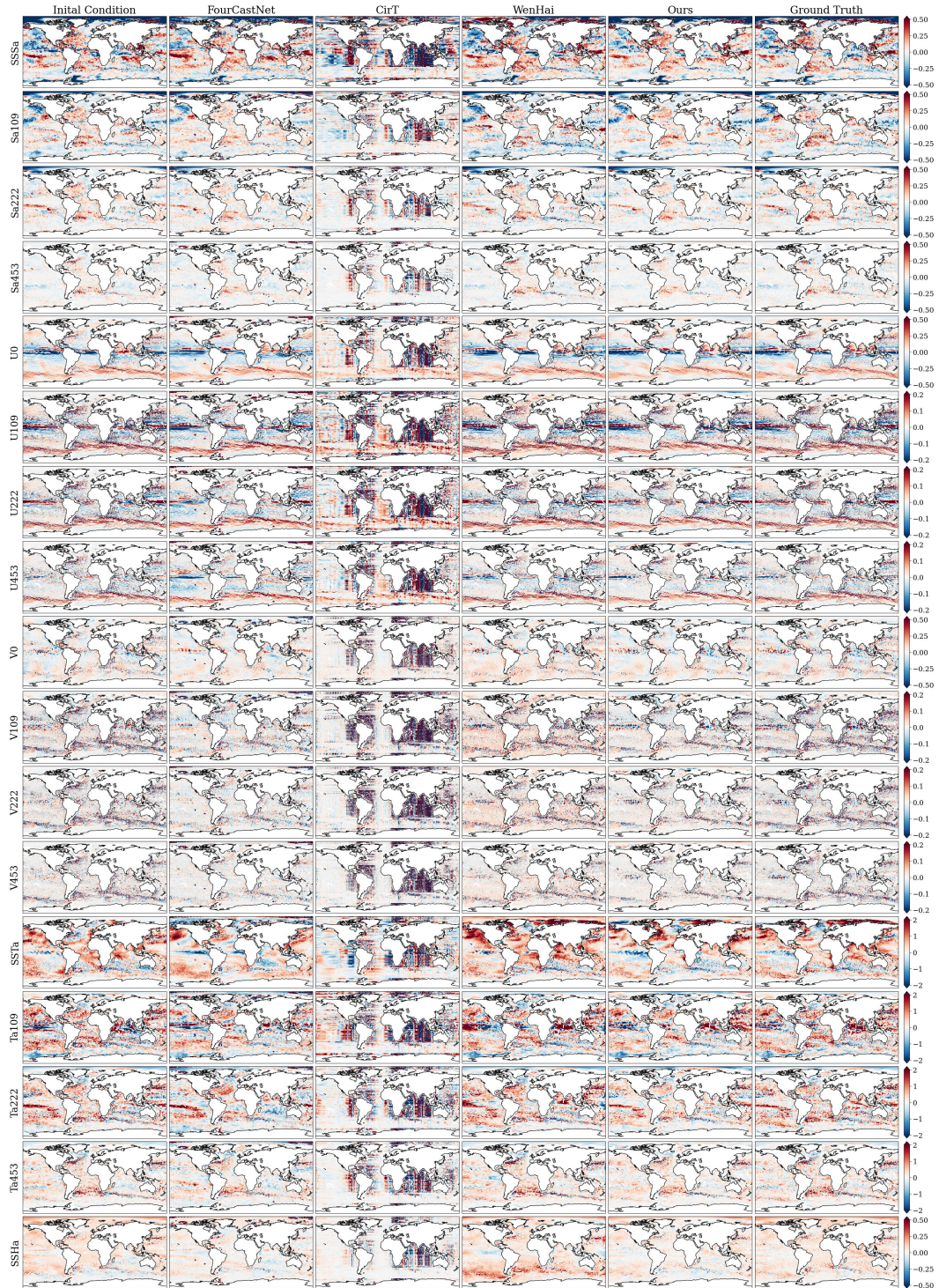


Figure 11: 60-day simulation results of different models.